Using prior shape and intensity profile in medical image segmentation

Conference Paper · November 2003

DOI: 10.1109/ICCV.2003.1238474 · Source: IEEE Xplore

6 authors, including:

Yunmei Chen
University of Florida
94 PUBLICATIONS **3,713** CITATIONS

SEE PROFILE

Murali Rao
GMR Institute of Technology
64 PUBLICATIONS **2,497** CITATIONS

SEE PROFILE

Feng Huang
71 PUBLICATIONS **2,184** CITATIONS

SEE PROFILE

Using prior shape and intensity profile in medical image segmentation

Yunmei Chen[1], Feng Huang[2] Hemant D. Tagare[3],
Murali Rao[4], David Wilson[5], Edward A. Geiser[8]

[1,2,4,5] Department of Mathematics, University of Florida, Gainesville, Fl. 32611

[3] Department of Diagnostic Radiology and Department of Electrical Engineering, Yale University, New Haven, CT. 06520

[6] Division of Cardiology, Department of Medicine, University of Florida, Gainesville, FL32610

[1,2,4,5][yun,feng,rao,dcw]@math.ufl.edu, [3]hemant.tagare@yale.edu [6] Geiseea@medicine.ufl.edu

Abstract

In this note we present a coupled optimization model for boundary determination. One part of the model incorporates a prior shape into a geometric active contour model with a fixed parameter. The second part determines the 'best' parameter used in the first part by maximizing the mutual information of the image geometry between the prior and an aligned novel image over all the alignments, that are the solutions of the first part corresponding to different parameters. We also present an alternative method, which generates an intensity model formed as the average of a set of aligned training images. Experimental results on cardiac ultrasound images are presented. These results indicate that the proposed model provides close agreement with expert traced borders, and the parameter determined in this model for one image can be used for images with similar properties. The existence of a solution to the proposed minimization problem is also discussed.

1 Introduction

In numerous medical imaging modalities, the boundaries of anatomical structures cannot be detected by algorithms that only use edge or region information. Reasons for this problem include significant signal loss, noise, and non-uniformity of regional intensities. These problems are ever present for images acquired in cardiac ultrasound, where the boundary detection problem is further complicated by the presence of confusing anatomical structures. In some cases, an image sequence may even have portions of the myocardium that lie outside of the sector scan so that some segments of its boundary may not be visible at all.

In an effort to overcome these difficulties, various techniques have been developed to incorporate prior information into the segmentation process. In [**?**] and [**?**], a statistical shape model was constructed from a set of corresponding points across the training images. This information was used in a Bayesian formulation to find the object boundary. In [**?**] a Gaussian model was fit to a training set of corresponding feature points. In [**?**] mixed models were used to fit to the data for specific applications where the distributions are non-Gaussian. In an alternate approach in [**?**], Staib and Duncan specified the shape of the curve by creating statistical priors on the Fourier coefficients of the contour. This prior was incorporated into segmentation processing in a Bayesian framework. Szekely, et. al. [**?**] also developed Fourier parameterized shape models, where an elastic fit of of the shape model in the subspace of eigenmodes was used to restrict the deformations. In an another approach, Tagare [**?**] matched shape templates to a boundary in an image. In [**?**] a method of deformable templates was proposed for feature extraction from faces. The features of the interest were described by a parameterized template which interacts dynamically with the image to minimize the energy function. More deformable models in medical image segmentation can be found in [**?**].

Recently, statistical shape knowledge has been incorporated in edge based or region based active contours. Leventon, et al. [**?**] extended geometric active contour methods developed in [**?**, **?**] by incorporating shape information into the evolution process. A principal component analysis was used to form a statistical shape model from a training set represented by using signed distance functions. A segmentation result was obtained by first involving the interface to capture image gradient, and then a correction was made by maximizing a posterior estimate of shape and pose. Chen, et al. [**?**] presented a variational technique to incorporate shape information into the geodesic active contours, The basic idea of their model is the creation of a shape term in the energy of the geodesic active contour, so that the propagation of the active contour stops when it arrives at high image gradients. and forms a shape similar to the prior. The shape term also recovers a similarity transformation that aligns the interface to the prior shape. Shape prior has also been used

Proceedings of the Ninth IEEE International Conference on Computer Vision (ICCV 2003) 2-Volume Set
0-7695-1950-4/03 $17.00 © 2003 IEEE

in region based segmentation schemes. For example, Cremers, et al. [**?**] incorporated statistical shape knowledge into the Mumford-Shah segmentation scheme [**?**] by adding a shape term to the Mumford-Shah energy functional. Tsai, et al. [**?**] designed a segmentation technique based on a parametric shape model, where the parameters are calculated to minimize a region based objective function.

Besides using shape prior, Leventon, et al. [**?**] incorporated intensity and curvature priors to segmentation process by an approach similar to the one he developed in [**?**].

While experimental results have shown the effectiveness of prior-based models in numerous medical applications, many problems remain including the complexity and variability of the images, the accuracy of the measurements obtained, and the rapid computation times required by the user. One practical problem is how to determine the parameter that balances the influences from image information and priors. If the evolution of an active contour is mainly governed by the force depending on the image gradient, it may be sensitive to the initial step or may leak through the boundary where the edge feature is not clearly defined. Conversely, if the force depending on the shape prior is the dominating term, the active contour may not arrive at the boundary of the object of interest even though it has a shape similar to the prior.

In this paper we propose to use prior intensity profiles to assist the determination of a parameter that balances the influence from image information and shape priors. The basic idea is to find the 'best' balance of the forces that govern the evolution of an active contour so that the active contour arrives at high gradients, forms a shape similar to the prior, and captures the prior intensity profile. Our approach is to solve a coupled optimization problem. The solution of the first problem minimizes an energy functional, that consists of two terms depending on image gradient and a prior shape with respectively with a parameter balancing these two terms. This solution provides a segmentation and a transformation that aligns the interface to the prior shape. The solution of the second problem maximizes the mutual information of image geometry (see the definition in section 2) between the prior image and the aligned novel image over all the alignments, that are the solutions of the first problem. The solution of the second problem provides an optimal estimate for the parameter used in the first problem, and hence obtain a desirable segmentation. The proposed model indeed performs segmentation and registration simultaneously. The registration in our model combines both a rigid transformation and a local deformation. The rigid motion is determined explicitly by shape matching, while the local deformation is determined implicitly by the image gradient and prior intensity profile. This idea is similar to the ideas used in [**?**, **?**, **?**] for matching nonequivalent shapes, where the authors consider a general deformation as the composition of a group action (rigid or affine transformation) and a local deformation.

Another reason to use prior intensity profiles to assist segmentation is that in some cases information of only the expected shape may not be sufficient to guide the active contour to the boundary of the object of interest. For instance, in some 2-chamber cardiac ultrasound images, the image intensities of the myocardium are non-uniform, a significant portion of the border appears at low contrast, and their shapes are not similar to the prior. For this class of images a model incorporating only prior shape in the active contours may not be able to give an accurate segmentation.

In this paper, we also present an alternative method for generating *average* intensity profiles from a set of training images. To generate an intensity model in [**?**] a Gaussian model was used to compute the joint distribution of the intensity values and signed distances to the boundary from a set of segmented training images. In ultrasound images signal is partially in the form of speckle ([**?**]). Since the statistics of speckle are non-Gaussian. modeling the randomness of ultrasound images using a Gaussian model is not appropriate. Our method of generating an intensity model is model free and based on maximizing mutual information of image geometry between the intensity model and aligned training images.

We report experimental results on apical 2-chamber echocardiographic images. We show that with appropriate prior shapes and intensity profiles, our technique is capable of finding boundaries in images that are complicated by significant signal loss, poor signal to noise ratio, and non-uniformality of intensities. Moreover, our experiments indicate that the proposed model is not too sensitive to either the initial step or the optimized parameter. Finally, the existence problem for our model is discussed at the end of the paper.

2 Model description

(1). Shape model:

The notion of shape in our model is assumed independent of translation, rotation, and scaling. The shape model C^* used in our algorithm was obtained by averaging the aligned training contours with similar shapes. The alignment of two contours C_1 and C_2 was made by finding a scale μ_j, a rotation matrix R_j, and a translation vector T_j such that the overlap area between the interiors of C_1 and $\mu R C_2 + T$ was maximized. In the case when the sample curves have large shape variations, a clustering process was required to group the training contours into several clusters. Then we created shape priors for each cluster as mentioned above. The details are available in [**?**].

(2). The Intensity model:

We now construct an *average* intensity profile across an

Proceedings of the Ninth IEEE International Conference on Computer Vision (ICCV 2003) 2-Volume Set
0-7695-1950-4/03 $17.00 © 2003 IEEE

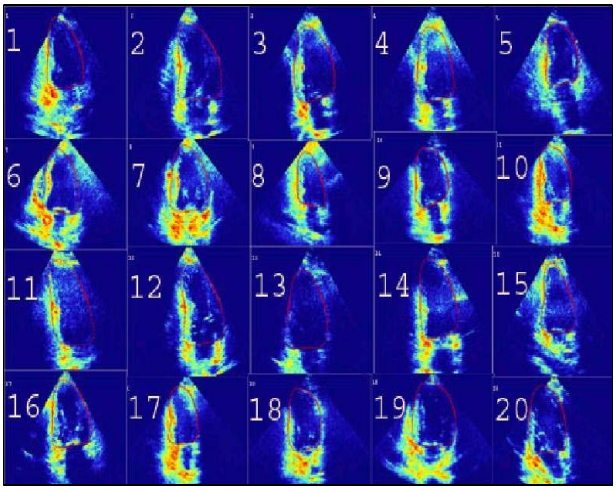

(a)

Figure 1: 20 training images segmented expert epicadial borders

average shape using the training images.

Let $C_i(p)$ $(i = 1, \ldots, m)$ be a set of training segmentations in one cluster, and I_i $(i = 1, \ldots, m)$ be the set of images associated with $C_i(p)$. Also, let $C^*(p)$ $p \in [0,1]$ be the *average* shape in this cluster. Our task is to generate an *average* intensity profile I^* across C^* from the training images. If I^* is created just by averaging all the sample images I_i $(i = 1, \ldots, m)$, I^* will most likely be blurred. To improve the quality of the averaged images, we select a subgroup from I_i $(i = 1, \ldots, m)$, in which the disparity in intensity profiles are relatively small. To do this, we first align each contour C_i $(i = 1, \ldots, m)$ to C^* by a similarity transformation (μ_i, R_i, T_i) that minimizes $a(C^*, \mu_i R_i C_i + T_i)$ defined in (2.1).

Next, we examine the similarity in the training intensity profiles across the training segmentations. Let

$$V_{\epsilon_0} = \{x \in \Omega | d(C^*, x) < \epsilon_0\}, \tag{2.2}$$

be a ϵ_0 neighborhood of C^*. If two images I_i and I_j are related approximately by

$$I_1(\mu_i^{-1} R_i^{-1}(x - T_i)) \simeq a I_2(\mu_j^{-1} R_j^{-1}(x - T_j)) + b \tag{2.3}$$

for some constants a and b, we may define the similarity measurement in the intensity profiles near the segmentations C_i and C_j by

$$\int_{V_{\epsilon_0}} |I(\mu_i^{-1} R_i^{-1}(x - T_i)) - a I_2(\mu_j^{-1} R_j^{-1}(x - T_j)) - b|^2 dx.$$

The integral is over V_{ϵ_0} rather than the entire image domain, since the intensity profiles near the segmentations are more meaningful. If the relation (2.3) is not valid, maximizing mutual information has been proven to be effective in solving matching problems, in particular in matching multi-modality images (see e.g. [**?**, **?**, **?**, **?**, **?**, **?**]). One of the advantages of using mutual information is that it does not require an explicit function that relates two images, but only assumes that aligned images explain each other better than when they are not aligned.

The mutual information between two random vectors X and Y is defined as:

$$MI(X, Y) = H(X) + H(Y) - H(X, Y),$$

where $H(Z) = -\int_{R^N} p(z) \log(p(z)) dz$ is the Shannon entropy of a random N-vector Z with density $p(z)$, and $H(X, Y) = -\int_{R^N} \int_{R^N} p(x, y) \log(p(x, y)) dx dy$ is the joint entropy of X and Y with joint density $p(x, y)$. If I_i and I_j are two images in the training set, then let $f(x) = I_i(\mu_i^{-1} R_i^{-1}(x - T_i))$ and $g(x) = I_j(\mu_j^{-1} R_j^{-1}(x - T_j))$. The *common* mutual information (MI) of I_i and I_j on V_{ϵ_0} is

$$MI_{V_{\epsilon_0}}(I_i, I_j) = \int_{R^2} p(f, g)(i_1, i_2) log \frac{p(f, g)(i_1, i_2)}{p(f)(i_1) p(g)(i_2)} di_1 di_2. \tag{2.4}$$

where $p(f, g)$, $p(f)$ and $p(g)$ are computed on V_{ϵ_0}. An extension of the *common* mutual information is called the *mutual information of image geometry* (MIIG). By MIIG of I_i and I_j on V_{ϵ_0}, we mean that $MIIG_{V_{\epsilon_0}}(I_i, I_j)$ is equal to the RHS of (2.4) with $f(x)$, $g(x)$, i_1 and i_2 replaced by the vectors $< f(x-2h), f(x-h), f(x), f(x+h), f(x+2h) >$, $< g(x-2h), g(x-h), g(x), g(x+h), g(x+2h) >$, $< i_1, i_2, i_3, i_4, i_5 >$ and $< i_6, i_7, i_8, i_9, i_{10} >$, respectively. The integral in (2.4) is computed over R^{10}.

Note that if the locations of two points in an image is switched, the intensity profile is changed, but the density function remains the same. Different from MI the MIIG uses the neighborhood intensity information, which gives better discription of the intensity profile at each point under the consideration. Therefore, in our algorithm we use the MIIG on V_{ϵ_0} as the measurement of disparity in intensity profiles,

The method was tested against one cluster of a database of 85 apical 2−chamber end diastolic (ED) echocardiographic images acquired retrospectively from 61 normal patients. The images were grouped into three clusters. The 20 images from one of the clusters with expert traced epicardial borders superimposed are displayed in Figure 1.

The *average* shape C^* for this cluster was also created by aligning their epicardial borders to the *average* shape C^*. The neighborhood V_{ϵ_0} was computed as a three pixel neighborhood of C^*. By using $MIIG_{V_{\epsilon_0}}(I_i, I_j)$ as the distance function in the k-means clustering algorithm, we formed a subgroup of 11 images, which are displayed as the first 11 images in Figure 1.

Proceedings of the Ninth IEEE International Conference on Computer Vision (ICCV 2003) 2-Volume Set
0-7695-1950-4/03 $17.00 © 2003 IEEE

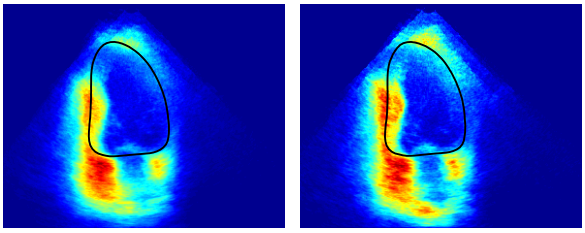

(a) (b)

Figure 2: (a) apical 2-chamber average images at ED from 20 normal patients with the *average* contour. (b) 2-chamber *average images* for the same 20 images generated by the proposed method with the *average* contour.

Denoting the subgroup of 11 images by $I_1, \ldots, I_{11}$, we now describe the construction of the *average* intensity profile I^* across C^* by

$$\max_{I^*} \sum_{j=1}^{11} MIIG_{V_{\epsilon_0}}(I^*, I_j), \tag{2.5}$$

where $MIIG_{V_{\epsilon_0}}(I^*, I_j)$ is defined as above and $f = I^*$ and $g = I_j(\mu_j^{-1} R_j^{-1}(x - T_j))$. Since this formulation is computationally intensive, we restricted ourselves to the cases where

$$I^* = \sum_{j=1}^{11} a_j I_j(\mu_j^{-1} R_j^{-1}(x - T_j)), \tag{2.6}$$

and found the weights a_j by using (2.5). We applied this method to the 20 training images in Figure 1, and obtained the *average* intensity profile I^* shown in Figure 2b. Moreover, we computed the sum in (2.5) for the weighted and unweighted ($a_j = 1/11$) average. The results were 196.73 and 184.08 respectively, confirming our suspicion that the weighted average is better.

(3). Segmentation with Priors:

We now present our variational approach for segmentation using both prior shape and intensity profile information. The key point of our model is to propagate a curve/surface by a velocity that depends on the image gradients, prior shape, and intensity profile. Thus, the propagation stops when the active contour/surface forms a shape similar to the shape prior, arrives at high gradients, and captures the prior intensity profile.

To begin the description of the proposed model, we first briefly review the active contour with a shape prior in [**?**]. Let $C^*(p)$ $(p \in [0, 1])$ be a curve representing the shape prior. The model in [**?**] minimizes the energy functional $E(C, \mu, R, T)$ defined as

$$\int_0^1 \{g(|\nabla I|)(C(p)) + \frac{\lambda}{2} d^2(C^*, \mu R C(p) + T)\} |C'(p)| dp, \tag{2.7}$$

where (μ, R, T) are similarity transformation parameters, $d(C^*, (x, y))$ is the distance from the point (x, y) to the curve C^*, and $g(|\nabla I|) = \frac{1}{1+\beta |\nabla G_\sigma * I|^2}$, where $\beta > 0$ is a parameter and $G_\sigma(x) = \frac{1}{\sigma} e^{-\frac{|x|^2}{4\sigma^2}}$. The first term in (2.7) is the energy functional of a geodesic active contour [**?**, **?**], that measures the amount of high gradient under the trace of the curve. The second term is the shape related energy that measures the disparity in shape between the interface and the prior. The constant $\lambda > 0$ is a parameter that balances the influence from the image gradient and the prior shape. The curve C and the transformation parameters μ, R, and T evolve to minimize $E(C, \mu, R, T)$. At the stationary point, the contour C lies over points of high gradient in the image and forms a shape close to C^*. This model also provides estimates for a similarity transformation that aligns the interface to prior shape. A geometric active contour often "leaks" through "gaps" in the boundary, which have low gradients, since it does not have any information about how the gaps are to be bridged. However, model (2.7) incorporates the information about the expected overall shape of the boundary in geometric active contours so that the active contour can compare its shape with the expected shape and bridge the gaps in a meaningful way. The experimental results in [**?**] showed model (2.7) is able to get a satisfactory segmentation in the presence of gaps as long as the boundary of the object of interest has a shape similar to the prior. However, this model still has problems. First, when the gaps are a substantial fraction of the overall boundary or when the shape of the boundary is substantially different from the prior, the model (2.7) will fail to provide an accurate segmentation, since insufficient information is available to decide how the gaps should be bridged. The second problem is to determine a value of the parameter λ in (2.7), which produces accurate segmentation.

To have a better solution to these two problems, we propose to incorporate both a prior shape and a prior intensity profile into the segmentation process. One method could be the creation of an intensity term in the energy functional (2.7), which minimizes the disparity between intensity profile and the prior shape across the interface:

$$\min_{C,\mu,R,T} \int_0^1 \{g(|\nabla I|(C(p))) + \frac{\lambda_1}{2} d^2(\mu R C(p) + T)\} |C'(p)| dp$$
$$-\lambda_2 GIMI_{V_{\epsilon_0}}(I^*(x), I(\mu^{-1} R^{-1}(x - T))), \tag{2.8}$$

where V_{ϵ_0} is defined in (2.2), C^* represents the prior shape, I^* represents the intensity profile, and $\lambda_1 > 0$ and $\lambda_2 > 0$ are parameters balancing the influences from the image

Proceedings of the Ninth IEEE International Conference on Computer Vision (ICCV 2003) 2-Volume Set
0-7695-1950-4/03 $17.00 © 2003 IEEE

gradient, prior shape, and prior intensity profile. By adding the third term in (2.7), the active contour governed by (2.8) is forced to arrive at a high gradient location, form a shape similar to the prior, and capture the prior intensity profile near the feature. However, the problem of determining the best choice of these parameters is not trivial.

In this paper we present an alternative approach that is not only able to incorporate both shape and intensity information into the segmentation process, but also able to provide an estimate for the parameter used in the model. Our model consists of a coupled optimization problem. The first problem is

$$\min_{C,\mu,R,T} E_\lambda(C,\mu,R,T),$$

with

$$E_\lambda(C,\mu,R,T) = \int_0^1 \{g(|\nabla I|)+\frac{\lambda}{2}d^2(\mu RC(p)+T)\}|C'(p)|dp. \tag{2.9}$$

The second problem is

$$\max_{\mu_\lambda,R_\lambda,T_\lambda} F(\mu_\lambda,R_\lambda,T_\lambda),$$

with

$$F(\mu_\lambda,R_\lambda,T_\lambda) = MIIG_{V_{\epsilon_0}}(I^*(x),I(\mu_\lambda^{-1}R_\lambda^{-1}(x-T_\lambda))), \tag{2.10}$$

where MIIG is the mutual information of image geometry defined in the second part of this section, and μ_λ, R_λ, and T_λ together with C_λ are the solutions of (2.9) corresponding to a fixed λ.

The energy functional in (2.9) is increasing in λ. Without the joint problem (2.10), E_λ in (2.9) takes the smallest value when $\lambda = 0$, that reduces to the energy functional for geometric active contour. It will leak through the boundaries with weak gradients. By maximizing the energy functional in (2.10) over all the possible solutions $(\mu_\lambda, R_\lambda, T_\lambda)$ of (2.9) corresponding to λ, we can get the 'best' estimate for λ, and hence a better segmentation corresponding to this optimal λ.

(4). The Level Set Form and EL Equations:

Level set methods [**?**] have been used extensively in active contour models because they allow for cusp, corners, and automatic topological changes.

Represent a contour C by the zero level set of a Lipschitz function u such that $\{x|u(x) > 0\}$ is the set inside C. Let $H(z)$ be the Heaviside function that is defined by: $H(z) = 1$ if $z \geq 0$, and $H(z) = 0$ if $z < 0$. If $\delta = H'(z)$ (in the sense of distribution) be the Dirac measure, then the length of the zero level set of u in the conformal metric $ds = g|C'(p)|dp$ can be computed by $\int_\Omega g|\nabla H(u)| = \int_\Omega \delta(u)g|Du|$. If the similarity of the shapes between the zero level set of u and C^* is evaluated by $\int_\Omega \delta(u)d^2(\mu Rx+T))dx$, then the level set formulation of (2.9) is given by

$$\min_{u,\mu,R,T} \int_\Omega \delta(u)\{g(|\nabla I|) + \frac{\lambda}{2}d^2(\mu Rx+T)\}|\nabla u|. \tag{2.11}$$

The evolution equations associated with the Euler-Lagrange equations of (2.11) are

$$\frac{\partial u}{\partial t} = \delta(u)div\{(g+\frac{\lambda}{2}d^2)\frac{\nabla u}{|\nabla u|}\}$$

$$\frac{\partial u}{\partial n} = 0,\ on\ \partial\Omega,\ t>0, \tag{2.12}$$

$$\frac{\partial \mu}{\partial t} = -\lambda\int_\Omega \delta(u)d\nabla d\cdot(Rx)|\nabla u|dx \tag{2.13}$$

$$\frac{\partial \theta}{\partial t} = -\lambda\int_\Omega \delta(u)\mu d\nabla d\cdot(\frac{dR}{d\theta}x)|\nabla u|dx, \tag{2.14}$$

$$\frac{\partial T}{\partial t} = -\lambda\int_\Omega \delta(u)d\nabla d|\nabla u|dx, \tag{2.15}$$

where R is the rotation matrix in terms of the angle θ, d is evaluated at $\mu Rx+T$.

3 Numerical Method and Experimental Results

We used the level set form (2.11) in our experiments. The minimization problem (2.11) was solved by finding a steady state solution of (2.12)-(2.15)while the equation (2.12) was implemented by the following iterative scheme:

$$\frac{u_{i,j}^{n+1}-u_{i,j}^n}{\Delta t} = \frac{1}{h^2}\delta_\epsilon(u_{i,j}^n)$$

$$\{\Delta_-^x(\frac{A_{ij}^n\Delta_+^x u_{i,j}^{n+1}}{\sqrt{(\Delta_+^x u_{i,j}^n)^2/h^2+(u_{i,j+1}^n-u_{i,j-1}^n)^2/(2h)^2}})$$

$$+\Delta_-^y(\frac{A_{ij}^n\Delta_+^y u_{i,j}^{n+1}}{\sqrt{(\Delta_+^y u_{i,j}^n)^2/h^2+(u_{i+1,j}^n-u_{i-1,j}^n)^2/(2h)^2}}),\}$$

where

$$A_{ij}^n = g_{i,j}^n + \frac{\lambda}{2}{d_{i,j}^n}^2.$$

The function δ_ϵ is a smooth version of the Dirac δ function, and $u_{i,j}^n = u(n\Delta t, ih, jh)$. However, the problem of solving (2.10) efficiently still remains an open question. In our experiments we first solved (2.11) to get a sequence of solutions $(C_{\lambda_i},\mu_{\lambda_i},R_{\lambda_i},T_{\lambda_i})$ corresponding to a sequence of λ_i, $i = 1,\ldots,k$. We then computed $F(\mu_{\lambda_i},R_{\lambda_i},T_{\lambda_i})$ in (2.10) for each $1 \leq i \leq k$. In this computation we partitioned the intensities into 16 bins, and

Proceedings of the Ninth IEEE International Conference on Computer Vision (ICCV 2003) 2-Volume Set
0-7695-1950-4/03 $17.00 © 2003 IEEE

the discrete form of Shannon entropy was used to calculate the MIIG. If $F(\mu_{\lambda_j}, R_{\lambda_j}, T_{\lambda_j})$ is minimal, we assigned $C_{\lambda_j}, \mu_{\lambda_i}, R_{\lambda_i}, T_{\lambda_i}$ as our model solutions. In this way we could get an improved estimate for λ, and hence, a better segmentation, that captures high gradients, the shape prior, and the intensity profile. However, since the energy values in (2.10) was computed for only a finite number of λ's, the solution may not be optimal

We applied this algorithm to echocardiographic images acquired from the apical 2-chamber at ED. Even though portions of the myocardium lay outside the sector scan fpr some of these images, our task was to find the epicardial border.

To create the prior shape, epicardial boundaries were outlined by an expert echocardiographer on 85 images acquired at ED from 61 patients. Using the method described in section II(1), the boundaries were grouped into three clusters and the *average* shape of each cluster was computed. Using the method described in section II(2), the intensity profile for each *average* shape was computed. The *average* shape C^* and the associated *average* intensity profile I^* for one cluster is displayed in Figure 2b. (The images in this cluster are the 20 images displayed in Figure 1.)

To segment the epicardial border in a novel image displayed in Figure 3b, we used the *average* contour and intensity profile near the contour in Figure 2b as the priors. The active contour was initialized with the ellipse displayed in Figure 3a. Evolving the active contour using equations (2.12)-(2.15) with a fixed λ, we constructed a segmentation C_λ together with a similarity transformation $(\mu_\lambda, R_\lambda, T_\lambda)$. By varying λ we generated a sequence of solutions of (2.11). We chose the optimal value of λ to be the one maximizing (2.10). Finally, the solutions for the model (2.11) coupled with (2.10) were chosen as the solutions of (2.11) corresponding to this optimal λ.

The first column of the table displays 8 different values of λ. By the procedure described above we obtained $C_{\lambda_i}, \mu_{\lambda_i}, R_{\lambda_i}, T_{\lambda_i}, (i = 1, \ldots, 8)$. The third and the fourth columns present the $MI_{V_{\epsilon_0}}(I^*(x), I(\mu_{\lambda_i}^{-1} R_{\lambda_i}^{-1}(x - T_{\lambda_i})))$, and $MIIG_{V_{\epsilon_0}}(I^*(x), I(\mu_{\lambda_i}^{-1} R_{\lambda_i}^{-1}(x - T_{\lambda_i})))$, respectively. Since the 4^{th} column of this table is largest when $\lambda = 0.04$, we selected the solutions of (2.11) to correspond to this choice of $\lambda = 0.04$. The segmentation corresponding to this λ (solid) is shown in Figure 3b together with the expert traced border (dotted). The distance between the expert and algorithm generated borders are tabulated in column 2 of the table. It is defined as $\sum_{i=1}^{N} d_{C^*}(C(p_i))/N$, where d_{C^*} is the distance function of C^*, and $C(p)$ is our segmentation. The units of the distance are the numbers of the pixels that are sized at 0.62mm × 0.62mm. From this table we see that the segmentation corresponding to $\lambda = 0.04$ is the one having smallest distance and largest value of MIIG. This statement is not true for MI.

λ	dist	MI	MIIG
0.04	3.1142	1.8894	7.9971
0.20	3.2903	1.9192	7.9794
0.40	3.3552	1.9207	7.9698
2	3.3962	1.9579	7.9623
20	4.7160	1.9207	7.8914
40	6.6697	2.0133	7.7524
0.02	25.4498	0	0
0.004	26.2190	0	0

Figure 3 displays experimental results for three additional images, where the images in each row are the same. The segmentation in Figure 3b is the solution of (2.11) when $\lambda = 0.04$. The segmentation in Figure 3c is the solution of (2.11) when $\lambda = 20$. This figure provides visual confirmation of the results presented in the table.

To further test the method, we also used the same initial contour and the 'optimal' value $\lambda = 0.04$ on two additional images. The segmentation results are presented in Figures 3d-3g. The segmentations in the left and right columns are the solutions of (2.11) corresponding to $\lambda = 0.04$ and $\lambda = 20$, respectively. Comparing the results in the left column of Figure 3 with those in the right column, we observe that $\lambda = 0.04$ also provides reasonable segmentations in these two new images indicating that the 'optimal' estimate of λ from one image can possibly be used for other members of the cluster. Of course, the shapes of the object boundaries and their intensity profiles must be similar.

Appendix: Existence of the Minimum

To investigate the existence problem for the model (2.11) coupled with (2.10), we first rewrite (2.11) in the form

$$\min_{\chi_E, \mu, \theta, T} \int_\Omega \{g(|\nabla I|(x) + \frac{\lambda}{2} d^2(\mu R x + T)\} |D\chi_E|, \quad (A.1)$$

where χ_E is the characteristic function of $E = \{x \in \Omega | u(x) \geq 0\}$. This minimization is over all the characteristic functions of E in $BV(\Omega)$

Next we prove a lemma from which the existence of a set of solutions to (A.1) coupled with (2.10) follows.

Lemma: Let Y be a topological space, $A : R \times Y \to R$ and $B : Y \to R$ be functions satisfying the conditions:

(1). for each $\lambda \in R$, $A(\lambda, \cdot)$ is lower semi continuous (l.s.c), and coercive w.r.t. a metric on Y.

(2). for each $y \in Y$, $A(\cdot, y)$ is continuous.

(3). B is w.l.s.c. on Y.

Let $S_\lambda = \{y \in Y | A(\lambda, y) = \min_{z \in Y} A(\lambda, z)\}$. Then,

(1). S_λ is nonempty.

(2). For each compact set $K \subset R$, $\cup_{\lambda \in K} S_\lambda$ is compact in Y.

(3). There is a $\lambda_0 \in R$ and $y_0 \in S_{\lambda_0}$ such that

$$B(y_0) = \min_{\lambda, z \in S_\lambda} B(z).$$

Proceedings of the Ninth IEEE International Conference on Computer Vision (ICCV 2003) 2-Volume Set
0-7695-1950-4/03 $17.00 © 2003 IEEE

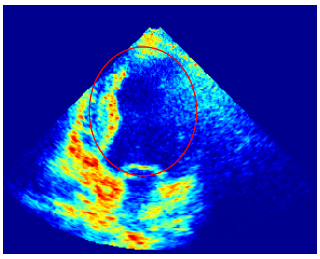

(a)

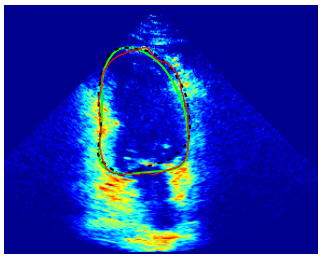

(b)

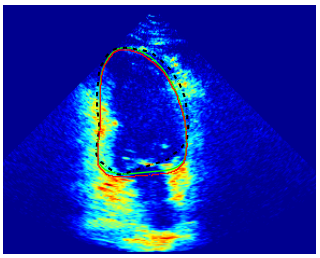

(c)

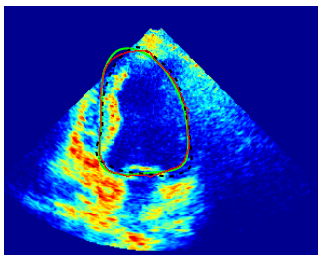

(d)

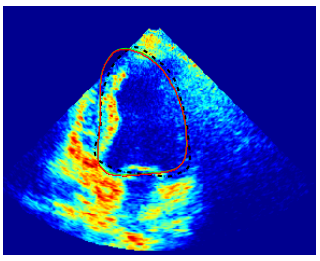

(e)

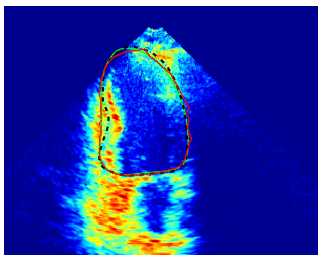

(f)

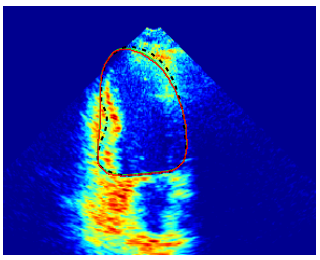

(g)

Figure 3: (a) An ellipse used as the initial contour in our expenments for three images in the following three rows. (b)-(g) Each row presents the segmentations (solid) and expert's borders (dotted) in an image. The segmentations in the left column and right column are the solutions of (2.11) corresponding to $\lambda = 0.04$ and $\lambda = 20$ respectively.

Proof:(sketch) The existence of a minimum for $A(\lambda, \cdot)$ on a compact set can be obtained by using condition (1). This implies that S_λ is nonempty. Moreover, if K is compact, $\lambda_n \in K$, and $y_n \in S_{\lambda_n}$, we may, by choosing subsequnces, if necessary, assume $\lambda_n \to \lambda_0$, $y_n \to y_0$. Then, $A(\lambda_0, y_0) \leq \liminf A(\lambda_n, y_n) \leq \liminf A(\lambda_n, z) = A(\lambda_0, z)$ for any $z \in Y$, showing that $y_0 \in S_{\lambda_0}$. This shows that $\cup_{\lambda \in K} S_\lambda$ is compact in Y. Furthermore, by lower semi continuity of B, B attains its minimum on this compact set, say at y_0. Such y_0 must belong to some S_λ concluding that

$$B(y_0) = \min_{\lambda, z \in S_\lambda} B(z).$$

By applying this lemma to $A =$ the energy functional in (A.1), $B =$ the energy in (2.10), and $y = (C, \mu, R, T)$ we get the following existence result:

Theorem: Let $\Omega \subset R^n$ be a bounded open set with a Lipschitz boundary. Let also C^* be a differentiable contour, and I^* and I are continuous on $\bar{\Omega}$. Then the problem (A.1) coupled with (2.10) has a solution $\chi_E \in BV(\Omega)$, $\mu \in (0, a]$, $\theta \in (-\pi, \pi]$, and $T \in [-a, a] \times [-a, a]$ for some $a > 0$ depending only on the size of Ω.

4 Conclusion

We proposed a coupling of shape and intensity driven segmentation method and applied to the problem of cardiac boundary determination in ultrasound images, for which the methods using edge or region information only can't give a good result. Even the active contours with shape prior struggle with such data.

The improvements of this model over existing active contour algorithms are in two aspects. First, we used maximizing MIIG rather than MI to match intensity profiles of two images. The reason for doing this is that MIIG takes neighborhood intensity pattern into account, while MI does not. Secondly, we proposed a coupling minimization framework to determine the optimal selection of the parameter in one of the minimization problems by minimizing the second problem over the solution set of the first one corresponding to different parameters. This idea can be used for the models with any three constraints.

The proposed model was tested against a database of epicardial borders traced by an expert on echocardiographic images acquired from the apical 2-chamber view. The preliminary results were encouraging. The existence of the solution to the proposed model was proved. However, much work needs to be done. The method will be tested against the entire database of normal images. and the images acquired from patients with some observable abnormality. We will also extend this model to 3-d cases.

Proceedings of the Ninth IEEE International Conference on Computer Vision (ICCV 2003) 2-Volume Set
0-7695-1950-4/03 $17.00 © 2003 IEEE

Acknowledgements

Y. Chen is supported by NIH grants P50-DC03888 and NS42075. H.D.Tagare is supported by the grant R01-LM06911 from the National Library of Medicine.

References

[CB] T. Cootes, C. Beeston, G. Edwards, and C. Taylor, "*Unified framework for atlas matching using active appearance models*", Int'l Conf. Inf. Proc. in Med. Imaging, Springer-Verlag, (1999), pp.322-333.

[CKS] V. Caselles, R. Kimmel, and G. Sapiro, " *Geodesic active contours*", IJCV, Vol.22(1), (1997), 61-79.

[CM] A. Collignon, F. Maes, D. Vandermeulen, P. Suetens, and G. Marchal, " Automated multimodality image registration using information theory", In Info. Processing in medical Images, Brest, France, (1995), 263-274.

[CT] T. Cootes and C. Taylor, "*Mixture model for representing shape variation*, Image and Vision Computing, 17(8) (1999), pp.567-574.

[CTC] T. Cootes, C. Taylor, D. Cooper and J. Graham, "*Active shape model - their training and application*, Computer Vision and Image Understanding, Vol. 61 (1995), pp. 38-59.

[CTT] Y. Chen, H. Tagare, S. R. Thiruvenkadam, F. Huang, D. Wilson, A. Geiser, K.Gopinath and R.Briggs, "*Using prior shapes in geometric active contours in a variational framework*, IJCV, Vol.50 (3), (2002), 315-328.

[CTW] D. Cremers, F. Tischh *a*user, J.Weickert, and C.Schn *o*rr, "*Diffusion-snakes: Introducing statistical shape knowledge into the Mumford-Shah functional* ", *International Journal of Computer Vision*, Vol.50 (3), (2002), pp. 295-315.

[CWH] Y. Chen, D. Wilson and F. Huang, "*A new procrustes methods for generating geometric models,*" Proceedings of World Multiconference on Systems, Cybernetics and Informatics, July 22-25, 2001, Orlando, (2001), 227-232.

[HCF] G. Hermosillo, C. Chefd'Hotel, and O. Faugeras, "*A variational methods for multimodal image matching*", IJCV, Vol.50 (3), (2002), 329-345.

[KS] S. Kichenassamy, A. Kumar, P. Olver, A. Tannenbaum, and A. J. Yezzi, "*Gradient flows and geometric active contour models*", Proc. ICCV'95, (1995), 810-815.

[LF] M. E. Leventon, O. Faugeras, E. Grimson, W. Wells. "*Level Set Based Segmentation with Intensity and Curvature Priors*" Mathematical Methods in Biomedical Image Analysis, (2000).

[LG] M. E. Leventon, E. Grimson, and O. Faugeras, "*Statistical Shape Influence in Geodesic Active Contours*", Proc. IEEE Conf. CVPR (2000), 316–323.

[MS] D. Mumford and J. Shah, "*Optimal approximation by piecewise smooth functions and associated variational problems*", Comm. Pure Appl. Math., Vol. 42, (1989), pp.557-685.

[MT] T. McInerney and D. Terzopoulous,"*Deformable models in medical image analysis: a survey*", Medical Image Analysis, Vol. 1(2), (1996), 91-108.

[OS] S. Osher and J. A. Sethian, "*Fronts propagating with curvature-dependent speed: algorithms based on Hamilton-Jacobi formulation*", J. Comp. Physics, Vol. 79 (1988), 12-49.

[PR] N. Paragios and M. Rousson, "*Shape prior for level set representations*", Computer Vision-ECCV2002, the 7th European Conference on Computer Vision, Copenhgen, Demark, May 2002 Proceeding.

[PRR] N. Paragios, M. Rousson, and V. Ramesh, *"Marching distance functions: a shape-to-area variational approach for global-to-local registration*", Computer Vision-ECCV2002, 775-789.

[SD] L. Staib and J. Duncan, "*Boundary finding with parametrically deformable contour methods*", IEEE Trans. Patt. Anal. and Mach. Intell., Vol. 14(11), 1992.

[SK] G. Szekely, A. Kelemen, C. Brechbuhler and G. Gerig, "*Segmentation of 2D and 3D objects from MRI volume data using constrained elastic deformations of flexible Fourier contour and surface models*", Medical Image Analysis, Vol.1(1),(1996), 199-234.

[SY] S. Soatto and A. Yezzi, "*Deformation: deforming motion, shape average and joint registration and segmentation of images*, Computer Vision-ECCV2002.

[T] H. D. Tagare, "*Deformable 2-D Template Matching Using Orthogonal Curves*," IEEE Trans. on Medical Imaging, vol. 16 (1), (1997) 108-117.

[TB] , Z. Tao, J. Beaty, C. C. Jaffe, and H. D. Tagare, "*Gary level models for segmenting myocardium and blood in cadiac ultrasound images*, Intl. Symp. on Biomedical Imaging, Washington D.C. July 2002.

[TY] A. Tsai, A. Yezzi,Jr., and A. S. Willsky, "*Curve evolution implementation of the Mumford-Shah functional for image segmentation, denoising, interpolation, and magnification*", IEEE Trans. on Image Proc., 10(8), (2001), 1169 -1186.

[TU] P. Thevenaz and M. Unser, "*Optimization of mutual information for multiresolution image registration*", IEEE Trans. on Image Proc., 9(12), (2000), 2083-2099.

[VW] P. Viola and W. M. Wells III, "*Alignement by maximization of mutual information*", IJCV, 24(2) (1997), 137-154.

[WCD] . W. Wells, A. Colchester, and S. Delp, editors. Number 1496 in Lecture Notes in Computer Science, Cambridge, MA, USA, (OCT.1998), Springer.

[WS] Y. Wang and L. Staih, *"Boundary funding with corresponding using statistical shape models"*, Proc. IEEE Conf. CVPR (1998), 338-345.

[WV] . W. M. Wells III, P. Viola, H. Atsumi, S. Nakajima, R. Kikinis, "*Multi-Modal Volume Registration by Maximization of Mutual Information*", Medical Image Analysis, 1(1), (1996), 35-51.

[YA] A. Yuille, P. W. Hallinan, and D. S. Cohen, "*Feature extration from faces using deformable templates*", IJCV, Vol.8, (1992), 99-111.

Proceedings of the Ninth IEEE International Conference on Computer Vision (ICCV 2003) 2-Volume Set
0-7695-1950-4/03 $17.00 © 2003 IEEE